INT. J. NUM. METH. HEAT FLUID FLOW, VOL. 6, NO. 6, 65–83 (1996)

A FINITE VOLUME METHOD FOR THE SOLUTION OF THE EXTRUDATE SWELL PROBLEM ON UNSTRUCTURED TRIANGULAR MESHES

G.K. DESPOTIS AND S. TSANGARIS

Laboratory of Aerodynamics National Technical University of Athens, PO Box 64070, 15710 Zografou, Athens, Greece

ABSTRACT

The extrudate swell phenomenon is analysed by solving, simultaneously, the Navier-Stokes equations along with the continuity equation by means of a finite volume method. In this work, the planar jet flows of incompressible viscous Newtonian and power-law fluids for Reynolds numbers as high as 75 are simulated. The method uses the velocity components and pressure as the primitive variables and employs an unstructured triangular grid and triangular or polygonal control volume for each separate variable. The numerical results show good agreement with previously reported experimental and numerical results. Shear thickening results in an increase in swelling ratio, while the introduction of surface tension results in a describes in swelling ratio.

KEYWORDS Navier-Stokes equations Unstructured finite volume Incompressible die-swell Power-Law model

INTRODUCTION

The flow of highly viscous fluids, such as a polymer melts, is commonly encountered in the materials-processing industry and many applications are conducted in the low-Reynolds-number regime. Such applications include pipe and profile extrusion which is used in the production of the rods, pipes, sheets and a wide variety of other final products. The extrusion process is not only of technological interest but also constitutes a challenging problem for numerical simulation owing to the presence of mixed boundary conditions. Once the fluid emerges from the die, it exhibits the characteristic phenomenon known as "extrudate swell" or "jet swell". Extrudate swell is most commonly given as the ratio of the extrudate dimension to the die dimension or as the change of extrudate dimension in reference to the die dimension expressed as a percentage. These definitions provide a quantitative measure of the swelling behaviour. The jet swell ratio is strongly dependent on the rheological properties of the liquid as well as other factors. Experimentally, the jet swell ratio has been found to be approximately 1.1-1.2 for Newtonian fluids[1-4].

Over the past 15 years numerous numerical studies of the jet swell problem have been undertaken and considerable progress has been realized with the steady improvement in computational hardware as well as software codes. Most of these numerical studies have employed finite element methods. Nickell *et al.*[3] first simulated creeping Newtonian jets and the kinematic condition was applied for free surface iteration. Omodei[5] later solved jet swell with surface tension effects. Ruschak[6] introduced a boundary location method so that the jet free surface was determined together with the flow field through a full Newton iteration. Georgiou *et al.*[7]

0961–5539

Received July 1994
Revised October 1994

applied the singular finite element method and accelerated the convergence on free surface iteration with mesh refinement.

On the other hand, very few numerical studies of the jet swell phenomenon have employed finite difference methods. Dutta and Ryan[8] examined the creeping Newtonian jet problem; the kinematic condition was used to update the free surface, and the jet swell ratios they obtained were closer to the finite element predictions than those of the previous finite difference studies. Liu *et al.*[9] extended the work of Dutta and Ryan[8] to study the planar Newtonian jet. They applied a numerical mapping technique, for co-ordinate transformation and they obtained solution for Reynolds numbers up to 100 and capillary number down to 0.1. Later Yu and Liu[10] modified the free surface iteration scheme of Liu *et al.*[9] and obtained numerical solutions as accurate as the finite elements simulations; however, the maximum Reynolds number in their study was still limited to 100.

In this paper, the planar jet flows of Newtonian and power-law fluids are simulated using a novel finite volume algorithm on unstructured triangular meshes. The Chorin fractional step method is used and the two dimensional, incompressible, viscous, laminar flows is simulated. The new element of this algorithm is that, while in the original Chorin method an explicit first order scheme in time is used and the spatial discretization depends on the finite difference mesh, now an implicit first order scheme in time is used and for the spatial discretization of the governing equations, a finite volume approximation on unstructured triangular mesh is applied.

Comparing with the finite element method (FEM), the finite volume method for unstructured grids (FVMUG) appears to have certain merits, such as: the mathematical formulation is easy and simulation for steady-state problems can be extended to time-dependent problems in a straightforward manner. The unstructured grid methods (FVMUG) have the distinct advantage over the structured grid methods (finite difference methods) in that they can easily treat the most complex of geometric configurations as well as the flow conditions, and that the unstructured grid can be moved to treat realistic motions and structural deformations of these configurations. This is the motivation of this paper.

The swelling of a creeping Newtonian jet was first selected as a test case. The convergent solution for the creeping Newtonian jet was used as the initial guess to produce numerical solutions for higher Reynolds number. Finally, in this work the effect of surface tension on the shape of a capillary jet for different values of the capillary number *ca* and the effect of the non-Newtonian behaviour on the shape of a jet for different values of the power-law index are presented.

MATHEMATICAL FORMULATION

Governing equations

The momentum and continuity equations of an incompressible viscous fluid are written in dimensionless form as,

$$\frac{\partial u_i}{\partial t} + \frac{\partial}{\partial x_j}(u_i\, u_j) = -\frac{\partial p}{\partial x_i} + \frac{1}{Re}\frac{\partial \tau_{i,j}}{\partial x_j} \tag{1}$$

$$\frac{\partial u_i}{\partial x_i} = 0 \tag{2}$$

where u_i denotes the velocity component in the x_i-direction in a Cartesian co-ordinate system, p is the pressure, Re is the Reynolds number of the flow and $\tau_{i,j}$ is the stress component. It should be noted that the convective terms in the momentum equation (1) are written in conservative form.

The equations have been normalized using a characteristic length L (defined as the half-channel width), a characteristic velocity U (defined as the average flow velocity) and a char-

acteristic viscosity $K(U/L)^{m-1}$, where K and m are the consistency index and power-law index respectively. The Reynolds number is denoted as $Re = \rho L^m U^{2-m}/K$. The pressure is normalized by ρU^2 and the stress terms by KU^m/L^m.

For the generalized Newtonian fluid the stress components are written as,

$$\tau_{xx} = 2\mu\frac{\partial u}{\partial x},\ \tau_{xy} = \mu\left(\frac{\partial u}{\partial y} + \frac{\partial v}{\partial x}\right),\ \tau_{yy} = 2\mu\frac{\partial v}{\partial y}$$

For a power-law fluid the viscosity is related to the second scalar invariant of the rate of deformation tensor as follows,

$$\mu = K\left|\frac{1}{2}\Pi\right|^{(m-1)/2} \tag{3}$$

where

$$\frac{1}{2}\Pi = 2\left[\left(\frac{\partial u}{\partial x}\right)^2 + \left(\frac{\partial v}{\partial y}\right)^2\right] + \left(\frac{\partial u}{\partial y} + \frac{\partial v}{\partial x}\right)^2. \tag{4}$$

The proposed method has been developed by Chorin[11]. In the explicit version of the fractional step method described by Chorin, an explicit first order scheme in time is used. The spatial discretization depends on the actual finite difference mesh that consists of quadrilateral elements. While Chorin used a non-staggered grid in his explicit version of the fractional step method, Andersson and Kristofferson[12] defined the dependent variables on the staggered grid positions with a similar implicit fractional step method. On the staggered grid the values of the velocities are evaluated at the middle of a cell's faces and the value of the pressure at the centre of the cell. This mesh distribution, is known as the M.A.C. mesh[13].

In the current fractional step method an implicit first order scheme in time is used with respect to the convective and diffusive terms. Now, the method is adapted to the basic equations (1) and (2) by splitting the former into two intermediate steps,

$$\frac{u_i^* - u_i^n}{\Delta t} + \frac{\partial}{\partial x_j}(u_j^n u_i^*) = \frac{1}{Re}\frac{\partial \tau_{i,j}^*}{\partial x_j} \tag{5}$$

$$\frac{u_i^{n+1} - u_i^*}{\Delta t} + \frac{\partial p^{n+1}}{\partial x_i} = 0 \tag{6}$$

where u_i^* is an intermediate, or tentative, value of the velocity component, $\tau_{i,j}$ is the stress components which is calculated as function of the tentative value of the velocity, and the superscript n denotes the solution at time $t = n\Delta t$, the time step being Δt. Thus, if the solution tends to a steady state, the velocity u_i^{n+1} at the new time level becomes equal to u_i^* according to (6).

An essential feature of the decomposition (5), (6) is that the tentative velocity u_i^* can be calculated implicitly from (5), while the new velocity u_i^{n+1} is related to the new pressure field p^{n+1} by (6). By taking the divergence of (6) and making subsequent use of the incompressibility condition (2) for u_i^{n+1}, we obtain the Poisson equation,

$$\frac{\partial^2 p^{n+1}}{\partial x_j\, \partial x_j} = \frac{1}{\Delta t}\frac{\partial u_i^*}{\partial x_i}. \tag{7}$$

Thus, with p^{n+1} known from the solution of (7), the velocities of the new time level $n + 1$ are readily derived from (6) as,

$$u_i^{n+1} = u_i^* - \Delta t\frac{\partial p^{n+1}}{\partial x_i}. \tag{8}$$

For the above mentioned test cases five types of boundaries are used: inflow boundary, outflow boundary, solid surfaces, symmetry axis and free surface. For each type and for each unknown let us see what boundary conditions are to be specified.

Boundary conditions

Boundary conditions for the velocities Inflow boundary

Inflow boundary

Here, a fully developed profile for the u-velocity is applied, while the v-velocity is set to be zero,

$$u = u(y) = \frac{2m+1}{m+1}(1 - y^{(m+1)/m})$$

$$v = 0$$

Outflow boundary

Here, the fully developed flow condition is applied,

$$\frac{\partial u}{\partial x} = \frac{\partial v}{\partial x} = 0$$

Symmetry axis

At the centreline the condition that is applied is the symmetry condition. Both the first order derivative of the u-component of the velocity in the y direction and the v-component of the velocity are set to be zero,

$$\frac{\partial u}{\partial y} = 0$$

$$v = 0$$

Solid surfaces

Here the non-slip condition is applied,

$$u = v = 0$$

Free surface

On the free surface, the following three conditions in dimensionless form must be satisfied,

(1) the kinematic condition

$$\frac{dH}{dx} = \frac{v}{u} \tag{9}$$

(2) the tangential stress balance

$$\left[1 - \left(\frac{dH}{dx}\right)^2\right]\left(\frac{\partial v}{\partial x} + \frac{\partial u}{\partial y}\right) - 2\frac{dH}{dx}\left(\frac{\partial u}{\partial x} + \frac{\partial v}{\partial y}\right) = 0 \tag{10}$$

(3) the normal stress balance

$$p\,Re - \frac{2\mu}{1 + (dH/dx)^2}\left[\left(\frac{dH}{dx}\right)^2 \frac{\partial u}{\partial x} + \frac{\partial v}{\partial y} - \frac{dH}{dx}\left(\frac{\partial v}{\partial x} + \frac{\partial u}{\partial y}\right)\right] + \frac{R}{C\alpha} = 0 \tag{11}$$

R is the dimensionless curvature that is defined as,

$$R = \frac{d^2H/dx^2}{[1 + (dH/dx)^2]^{3/2}}.$$

H is the dimensionless locations of the free surface and the capillary number is defined as $C\alpha = KU^m/\sigma L^{m-1}$ where σ is the surface tension coefficient.

The boundary conditions on the free surface (10) and (11) can be formulated explicitly as,

$$\frac{\partial u}{\partial y} = \frac{2dH/dx}{1-(dH/dx)^2}\left(\frac{\partial u}{\partial x} - \frac{\partial v}{\partial y}\right) - \frac{\partial v}{\partial x} \tag{12}$$

$$\frac{\partial v}{\partial y} = \frac{dH}{dx}\left(\frac{\partial u}{\partial y} + \frac{\partial v}{\partial x}\right) - \left(\frac{dH}{dx}\right)^2 \frac{\partial u}{\partial x} + \frac{1+(dH/dx)^2}{2\mu}\left(p\,Re + \frac{R}{C\alpha}\right). \tag{13}$$

These two equations are interchangeably used to eliminate the vertical gradient term on the right-hand side of each equation. Then the following form for the boundary conditions is obtained,

$$\frac{\partial u}{\partial y} = 2\frac{dH}{dx}\frac{\partial u}{\partial x} - \frac{\partial v}{\partial x} - \frac{dH/dx}{\mu}\left(p\,\mathrm{Re} + \frac{R}{C\alpha}\right) \tag{14}$$

$$\frac{\partial v}{\partial y} = \left(\frac{dH}{dx}\right)^2 \frac{\partial u}{\partial x} + \frac{1-(dH/dx)^2}{2\mu}\left(p\,\mathrm{Re} + \frac{R}{C\alpha}\right). \tag{15}$$

Boundary conditions for the pressure

Free surface

The boundary condition on the free surface can be formulated explicitly as,

$$\frac{\partial u}{\partial x} = \frac{1-(dH/dx)^2}{2dH/dx}\left(\frac{\partial u}{\partial y} + \frac{\partial v}{\partial x}\right) + \frac{\partial v}{\partial y}. \tag{16}$$

Equations (16) and (13) are interchangeable and are used to eliminate the vertical gradient term on the right-hand side of (16) and the axial gradient term on the right-hand side of (13), which then results in the following,

$$\frac{\partial u}{\partial x} = \frac{1}{2dH/dx}\left(\frac{\partial u}{\partial y} + \frac{\partial v}{\partial x}\right) + \frac{1}{2\mu}\left(pRe + \frac{R}{C\alpha}\right) \tag{17}$$

$$\frac{\partial v}{\partial y} = \frac{dH/dx}{2}\left(\frac{\partial u}{\partial y} + \frac{\partial v}{\partial x}\right) + \frac{1}{2\mu}\left(pRe + \frac{R}{C\alpha}\right). \tag{18}$$

The continuity equation after some manipulations with (17) and (18) yields an expression for calculation of the pressure on the free surface,

$$p = -\frac{1}{Re}\left\{\frac{\mu[1+(dH/dx)^2]}{2dH/dx}\left(\frac{\partial u}{\partial y} + \frac{\partial v}{\partial x}\right) + \frac{R}{C\alpha}\right\}. \tag{19}$$

Other boundaries

The boundary conditions imposed on p are consistent with (6). Thus, if we take

$$u_i^* = u_i^{n+1} \tag{20}$$

on a boundary with its normal along the x_i-direction, (8) becomes,

$$\frac{\partial p^{n+1}}{\partial x_i} = 0 \tag{21}$$

i.e. zero normal derivative of p^{n+1} on the boundary.

The boundary value problem given by the Poisson equation (7) subject to the Neumann boundary condition (21) is an interior Neumann problem, for three-dimensional case, for which,

$$\iiint_V \frac{\partial u_i^*}{\partial x_i} dV = 0 \tag{22}$$

is a necessary condition for a solution to exist. By using Gauss's theorem, the compatibility condition (22) becomes,

$$\iint_S u_i^* n_i \, dS = 0 \tag{23}$$

where n_i denotes the components of the unit normal vector to the boundary S of the calculation domain V. Thus, by introducing (20) in the surface integral (23), it is observed that compatibility is automatically achieved, provided that the boundary conditions on u_i^{n+1} assure zero net flux into the calculation domain.

Around the computational domain there are "pseudo-cells" that are used for the implementation of the boundary conditions. This is necessary because the pressure is calculated at the centre of the triangular cell and the flux terms are calculated across the edges of it.

THE NUMERICAL SOLUTION

Spatial discretization

In this work, the Navier-Stokes equations are integrated in time using an implicit first order time step scheme. These equations are integrated in space using a finite volume method that is developed for an unstructured grid made up of triangles[14]. For the integration around a finite volume, the derivatives of the flow equations must be converted into closed line integrals using some formulation of the Stokes theorem, that is described by the following equation,

$$\oint_S \vec{\alpha} \cdot d\vec{r} = \int_E rot\, \vec{\alpha} \cdot \vec{n} \, dE$$

where $d\vec{r}$ is the elementary arc, dE is the elementary surface and $\vec{n}$ is the normal vector to this surface.

A structured triangular grid – that is constructed using interpolations – is used for the numerical solution of the flow equations, but the current algorithm considers it as unstructured. For structured grids, mesh co-ordinate directions can be identified and used to number the cells and nodes. Thus, a cell may be identified by its two indices I and J in the mesh co-ordinate system, and its neighbours may be located by incrementing one of these indices. However, for unstructured meshes this no longer possible, since in principle the cells and nodes are ordered randomly. Thus, the use of unstructured meshes requires the storage of connectivity information along with the use of an indirect addressing system.

Since flux and diffusive terms are to be calculated at each point of the mesh, a data structure based on the mesh points can be employed. To define a point-based structure, IMAX = 3 × IE integer addresses must be stored for each point. IE is the number of the polygon's edges which surrounds the computational point c (See *Figure 1*). For example in *Figure 1* IE = 6. Thus, an array must be dimensioned KNU(KMAX × IMAX) where KMAX is the total number of points in the mesh. For each point, the first 2 × IE values in KNU, correspond to the addresses of the neighbouring points of that point, and the other IE values correspond to the addresses of the triangular cells which have that point as a common vertex.

On the triangular mesh the velocities are stored at the nodes of the triangular cell and the pressure at the centre of it. Using the finite volume technique on an unstructured triangular mesh the flux terms are calculated at the nodes and across the edges of the triangular cell and the diffusive terms at the nodes.

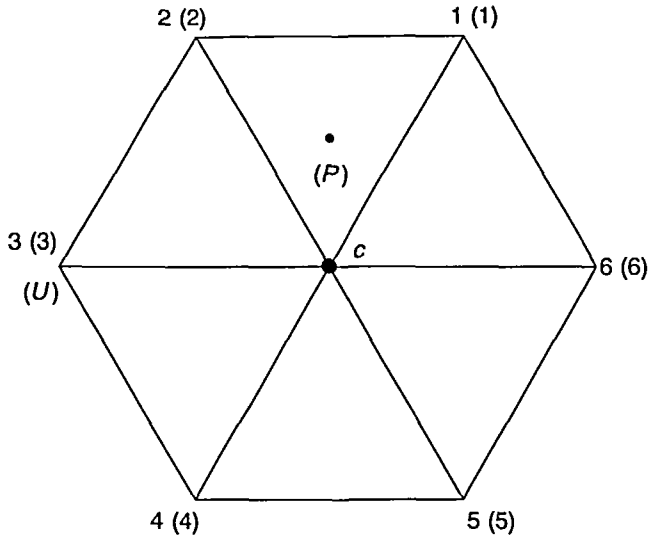

Figure 1 Equivalent control volume for a finite-volume approximation to the flux terms at polygon's centre

Two finite volumes are used (triangle and polygon) because the pressure is calculated at the centre of the triangular cell and the velocities at the nodes of it. Thus, two such finite volume discretization schemes have been adapted, the Cell-Centred scheme and the Nodal scheme.

Discretization of the flux terms at polygon's centre

In this case, the velocities are stored at the nodes of the polygon and the flux terms are calculated at the node c (See *Figure 1*). The Nodal finite volume discretization scheme[15] is used for the discretization of the flux terms that appear in the momentum equations (convective terms). The first differences are computed as,

$$\left(\frac{\partial U}{\partial x}\right)_c = \frac{1}{A_c}\int_{S_c} U dy = \frac{1}{A_c}\sum_{i=1}^{IE}\frac{U_{i+1}+U_i}{2}(y_{i+1}-y_i)$$

$$\left(\frac{\partial U}{\partial y}\right)_c = -\frac{1}{A_c}\int_{S_c} U dx = -\frac{1}{A_c}\sum_{i=1}^{IE}\frac{U_{i+1}+U_i}{2}(x_{i+1}-x_i).$$

A_c is the area of the polygonal control volume (1-2-3-4-5-6) (See *Figure 1*), U is the component of the fluxes and x, y are the co-ordinates of the polygon vertices, and i refers to the six vertices of the polygonal control volume.

In *Figures 1* to *5* the numbers out of the parentheses refer to the index of the equations and the numbers in the parentheses denote the same locations of *Figure 3*. In the same figures (P) and (U) denote the location of pressure and velocity nodes.

The closed line integral is approximated by the trapezoidal integration rule: for each edge delimiting the control volume boundary, the contribution to the closed line integral is obtained by evaluating the velocities at the nodes on both ends of the edge and taking the scalar product of their averaged value with the directed length of the edge. This discretization can be shown to be equivalent to a finite-element Galerkin approximation[15], which is known to be second-order accurate in space for a mesh that consists of equilateral triangles.

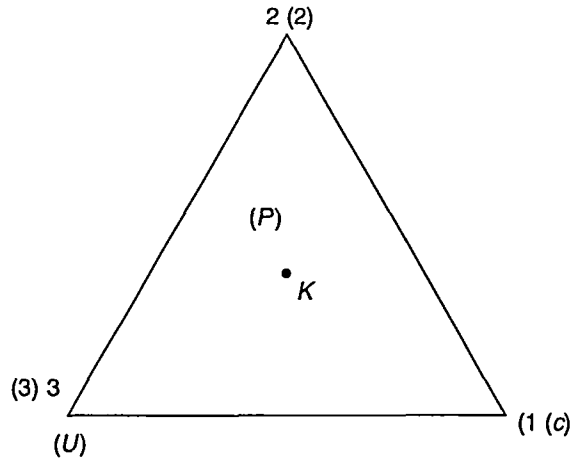

Figure 2 Equivalent control volume for a finite-volume approximation to the flux terms at triangle's centre

Discretization of flux terms at triangle's centre

In this case, the spatial discretization procedure begins by storing the velocities at the vertices of the triangular cells. The flux terms must be calculated at the centres of the triangles (see *Figure 2*). This is achieved by computing the required first differences for the velocities at the triangles' centres[16]. For a piecewise linear approximation of the velocities in the space, the first differences are constants over each triangle, and they are computed as:

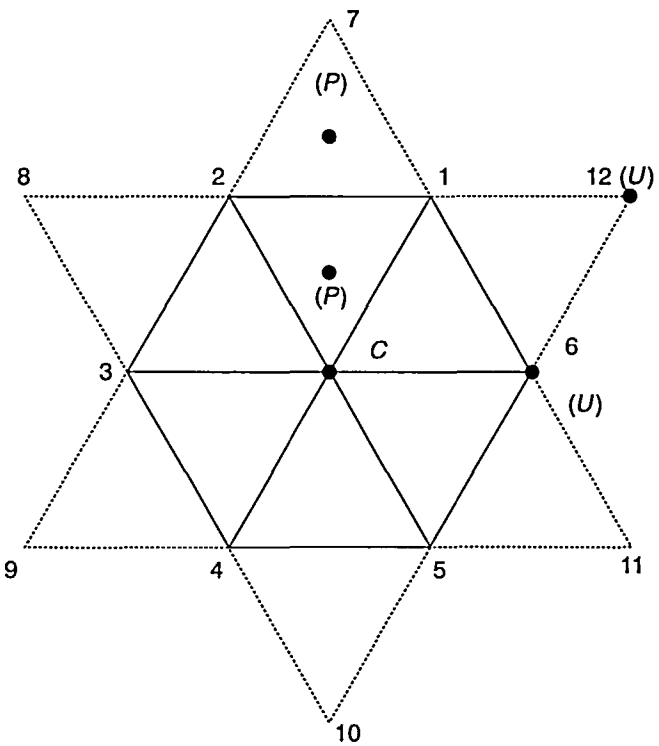

Figure 3 Equivalent control volume for a finite-volume approximation to the diffusive terms at polygon's centre

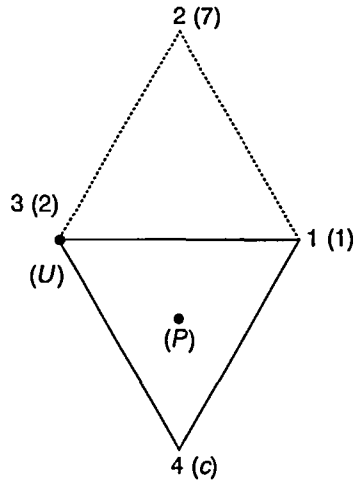

Figure 4 Equivalent control volume for a finite-volume approximation to the 1st order derivative of velocity at the middle of polygon's edge

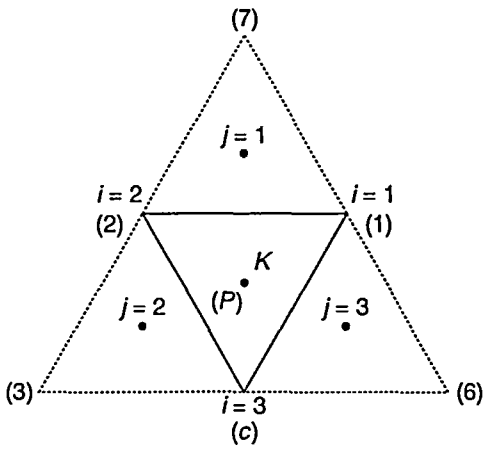

Figure 5 Equivalent control volume for a finite-volume approximation to the 1st and 2nd order pressure terms at triangle's centre

$$\left(\frac{\partial U}{\partial x}\right)_K = \frac{1}{A_K}\int_{S_K} U dy = \frac{1}{A_K}\sum_{i=1}^{3}\frac{U_{i+1}+U_i}{2}(y_{i+1}-y_i)$$

$$\left(\frac{\partial U}{\partial y}\right)_K = -\frac{1}{A_K}\int_{S_K} U dx = -\frac{1}{A_K}\sum_{i=1}^{3}\frac{U_{i+1}+U_i}{2}(x_{i+1}-x_i)$$

A_K is the area of the triangular control volume (1-2-3) (See *Figure 2*), U is the component of the velocity and the summation over i refers to the three vertices of the triangle.

Generally, the nodal finite volume scheme is used for the discretization of the flux terms that appear in the right hand side of the Poisson equation, but in this case the control volume is not polygonal but triangular. The closed line integral is approximated in the same manner as referred to previously.

Discretization of diffusive terms at polygon's centre

The spatial discretization procedure begins by storing the velocities at the vertices of the polygon (1-2-3-4-5-6) and at the vertices of the neighbouring triangles (See *Figure 3*). The diffusive terms must be calculated at the node c, and this is achieved by computing the second order derivatives at the same point. The required second differences may be computed as:

$$\left(\frac{\partial^2 U}{\partial x^2}\right)_c = \left[\frac{\partial}{\partial x}\left(\frac{\partial U}{\partial x}\right)\right]_c = \frac{1}{A_c}\int_{S_c}\frac{\partial U}{\partial x}dy = \frac{1}{A_c}\sum_{i=1}^{IE}\left(\frac{\partial U}{\partial x}\right)_{i+1/2}(y_{i+1}-y_i)$$

$$\left(\frac{\partial^2 U}{\partial y^2}\right)_c = \left[\frac{\partial}{\partial y}\left(\frac{\partial U}{\partial y}\right)\right]_c = -\frac{1}{A_c}\int_{S_c}\frac{\partial U}{\partial y}dx = -\frac{1}{A_c}\sum_{i=1}^{IE}\left(\frac{\partial U}{\partial y}\right)_{i+1/2}(x_{i+1}-x_i).$$

A_c denotes the area of the polygonal control volume, U denotes the component of the velocity, i refers to the six vertices of the polygon and $i + 1/2$ refers to the six middles of the edges of the polygon.

The viscous components involve the evaluation of derivatives of the primitive variables (velocities) on each polygonal contour. To be consistent with the overall contour integral method of evaluating derivatives, it remains to define a suitable contour for obtaining first derivatives on edges. There is no unique way to perform the integration, but perhaps the simplest is to use the contour shown in *Figure 4*, so that the derivative at the middle of the edge is the sum of four terms[17]. The first differences at the middle of the edge are defined as,

$$\left(\frac{\partial U}{\partial x}\right)_{i+1/2} = \frac{1}{A}\int_S U dy = \frac{1}{A}\sum_{j=1}^{4}\frac{U_{j+1}+U_j}{2}(y_{j+1}-y_j)$$

$$\left(\frac{\partial U}{\partial y}\right)_{i+1/2} = -\frac{1}{A}\int_S U dx = -\frac{1}{A}\sum_{j=1}^{4}\frac{U_{j+1}+U_j}{2}(x_{j+1}-x_j)$$

where, A is the sum of the areas of the two adjacent triangles which define the contour, U is the velocity component and the summation over j refers to the four vertices of the quadrilateral.

The Nodal finite volume scheme, which is used for discretization of the first and second differences and the overall contour integral, is approximated in the same way as referred to previously.

Discretization of 1st order pressure terms at triangle's centre

The Cell-Centred finite volume scheme[18] is used for discretization of the first order pressure terms, which are calculated at the centre of the triangular control volume (1-2-3) (See *Figure 5*). The first differences defined as,

$$\left(\frac{\partial P}{\partial x}\right)_K = \frac{1}{A_K}\int_{S_K} P dy = \frac{1}{A_K}\sum_{i-j=1}^{3}\frac{P_K+P_j}{2}(y_{j+1}-y_j)$$

$$\left(\frac{\partial P}{\partial y}\right)_K = \frac{1}{A_K}\int_{S_K} P dx = -\frac{1}{A_K}\sum_{i-j=1}^{3}\frac{P_K+P_j}{2}(x_{j+1}-x_j).$$

A_K denotes the area of the triangular control volume, P denotes the pressure, i refers to the three vertices of triangular cell and j refers to the centres of the three neighbouring triangles.

The pressure is stored at the centre of each cell and assumed to represent an average value over the entire control volume. In order to evaluate the closed line integral, estimates of the pressure along the edges of the triangular cell are needed. These are taken as the average of the values at both cells on either side of that edge. This is the equivalent of central differencing on a Cartesian grid and is second order accurate for a mesh that consists of equilateral triangles.

Discretization of 2nd order pressure terms at triangle's centre

The second order pressure terms that appear in the left hand side of Poisson equation, are also calculated at the centre K of the triangular control volume (1-2-3) (See *Figure 5*). These calculations require the evaluation of second differences of pressure at the same point K. The second order derivatives of pressure may be computed as,

$$\left(\frac{\partial^2 P}{\partial x^2}\right)_K = \left[\frac{\partial}{\partial x}\left(\frac{\partial P}{\partial x}\right)\right]_K = \frac{1}{A_K}\int_{S_K}\frac{\partial P}{\partial x}\,dy = \frac{1}{A_K}\sum_{i-j=1}^{3}\frac{(P_x)_K + (P_x)_j}{2}(y_{i+1} - y_j)$$

$$\left(\frac{\partial^2 P}{\partial y^2}\right)_K = \left[\frac{\partial}{\partial y}\left(\frac{\partial P}{\partial y}\right)\right]_K = -\frac{1}{A_K}\int_{S_K}\frac{\partial P}{\partial y}\,dx = \frac{1}{A_K}\sum_{i-j=1}^{3}\frac{(P_y)_K + (P_y)_j}{2}(x_{i+1} - x_j)$$

where, A_K, P, i, j are the same as referred to previously and P_x and P_y are the x and y first order derivatives of pressure, respectively.

For the evaluation of second differences of pressure, the Cell-Centred finite volume discretization scheme is also used but the first order derivatives of pressure must be known. These can be evaluated as outlined previously.

Numerical procedure

The numerical procedure for solving the jet flow problem consists of two steps, as follows:

(I) Solution of the flow equations

The procedure for solving the flow equations is given as follows.

1. An initial field for velocity and pressure is applied.
2. The momentum equations are solved and a velocity field, that does not fulfil the continuity equation, is obtained. The solutions of the momentum equations are obtained using the Gauss-Seidel method.
3. The Poisson equation is solved and a pressure field is calculated. The solution of the Poisson equation is also obtained using the Gauss-Seidel method.
4. The velocity components at the new time step level are evaluated from (6).

If the maximum difference between guessed values and newly generated values is smaller than a preset tolerance, then go to (II); otherwise return to step 2.

(II) Updating the free surface

With the converged solution of u and v on the free surface available, (9) is used to generate a new position of the free surface. Equation (9) can be integrated numerically starting from the separation point (x_{sp}) as follows,

$$H(x) = \sum_{x_{sp}}^{x-x_{sp}} \frac{v}{u}\,dx.$$

The trapezoidal rule is used to obtain $H(x)$. Once a new position of the free surface is generated, the convergence check is continued by comparing it with the current position of the free surface on each grid point in the physical plane. If convergence is achieved – i.e. the maximum difference of the two free surface positions is smaller than a preset value – the computation is complete; otherwise the current free surface position is updated and the iteration is repeated starting from (I).

RESULTS

The swelling of a creeping Newtonian jet was first selected as a test case. The convergent solution for the creeping Newtonian jet was used as the initial guess to produce numerical solutions for

high Reynolds number. *Figure 6* shows a part of the grid that is used for creeping flow and it consists of 1,979 nodes. For Reynolds number Re = 10, 30 and 75 similar grids that consist of 2,734, 3,184 and 4,534 nodes, respectively, are used. The upstream length was selected to be 3 for the range of Reynolds number that was studied. The downstream length was selected to be 12 for creeping flow and for Re = 10, 14.5 for Re = 30 and 22.for Re = 75. The location of the free surface, which can be computed by (II) in the previous section, was updated 24 times for creeping flow, 20 times for Re = 10, 18 times for Re = 30 and 15 times for Re = 75. The time steps used are Δt = 0.0008, 0.05, 0.16 and 0.34, respectively.

The shapes of the creeping Newtonian jet determined by different numerical approaches are given in *Figure 7*. All the authors found that the jet will reach its final thickness at a downstream length greater than 2, but the shapes for downstream length less than 2 are slightly different. The planar jet has a swelling ratio of 19.08 per cent and is considered to be in reasonable agreement with the experiments of Whipple and Hill[19] and the previous numerical predictions of 16.10 per cent[8], 18.80 per cent[20], 19.00 per cent[21], 19.60 per cent[22] and 19.10 per cent[23].

In *Figure 8* the steady u-component of the velocity is given at several x locations: x = 3.47, 3.98, 4.98, 7.00 and 10.02.

In *Figure 9* the free surface profiles have been illustrated graphically for three conditions: Re = 10, 30 and 75. The jet has a swelling ratio of –0.87 per cent for Re = 10, –9.86 per cent for Re = 30 and –11.68 per cent for Re = 75. As can been observed, the jet contracts as the Reynolds number increases.

Figure 10 gives the pressure profiles along the symmetry axis and the free surface for the creeping Newtonian jet and for Re = 10, 30 and 75. For the creeping flow of a Newtonian fluid the axial pressure gradient along the centreline decreases monotonically from the Poiseuille value to zero as the fluid traverses through the exit region. The surface pressure, on the other hand, shows a negative value (lower than the outer pressure) at the die exit and asymptotically approaches zero far downstream. If the Reynolds number is greater than 1 the axial pressure gradient along the centreline does not decrease monotonically. The axial pressure decreases from the Poiseuille value to a negative value of the die exit and asymptotically approaches zero far downstream. The behaviour of the surface pressure is analogous with the behaviour of the surface pressure of the creeping flow.

A comparison of the jet swell ratio with previous works[6,9,21,24] is given in Figure 11 (shown after the References). Co is the ratio of the extrudate dimension to the die dimension. Values of the jet swell ratio Co computed by the present method are close to those of finite element simulations[6,21,24] and are also close to that of finite difference simulations[9] if the Reynolds number is low. However, as the Reynolds number increases, the swell ratio predicted by the present method is about 6 per cent higher than previous work, that was based on the finite difference method.

The effect of surface tension on the jet free surface of Re = 1 is shown in *Figure 12* (shown after the References). As the surface tension increases, $C\alpha$ will decrease and the jet will have less swelling, even though the effect is not significant. Similar results for Re = 20 are given in *Figure 13*. Comparing with the jet shapes in *Figure 12*, the jet contracts now instead of swelling and the fluid surface tension tends to reduce the contraction. The effect of the surface tension on the jet shape appears to be less important as Reynolds number increases.

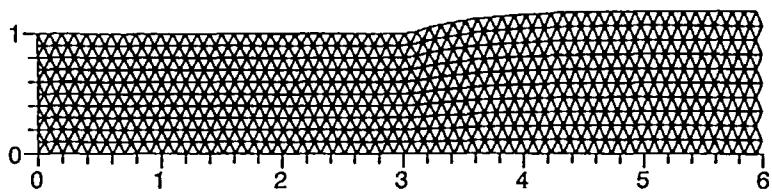

Figure 6 The shape and mesh of a creeping Newtonian jet

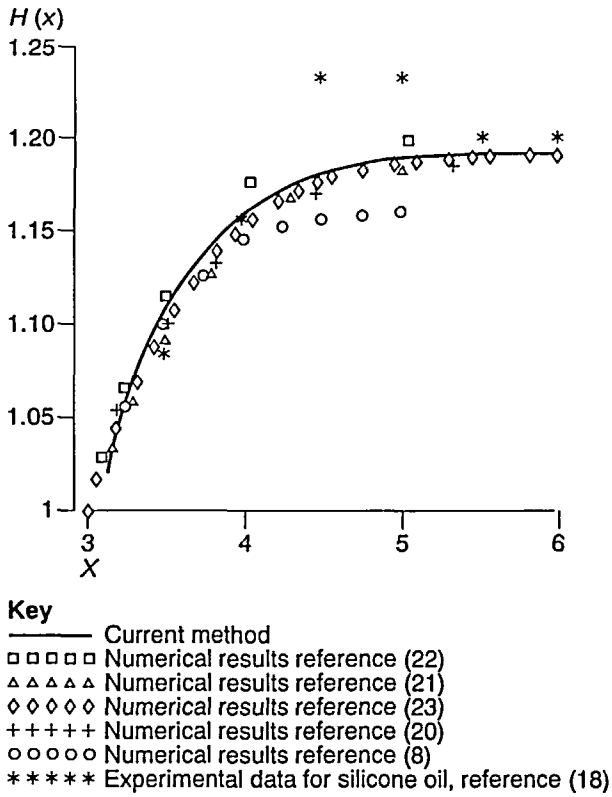

Figure 7 Comparison between numerical and experimental surface profiles for creeping Newtonian jets

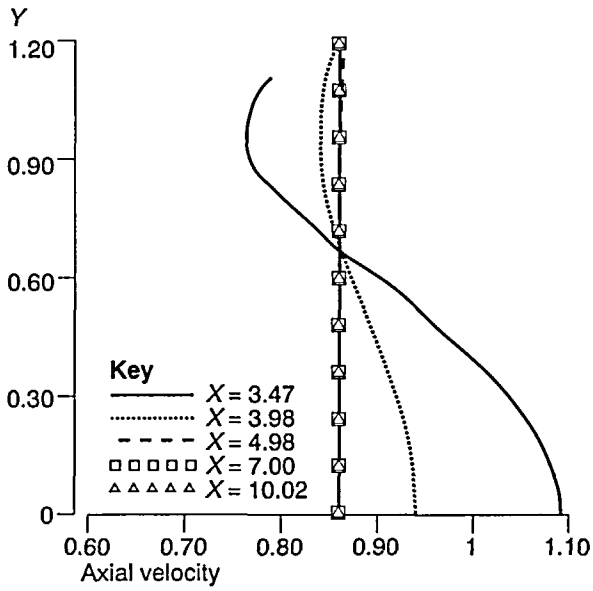

Figure 8 Axial velocity profiles for die-swell problem

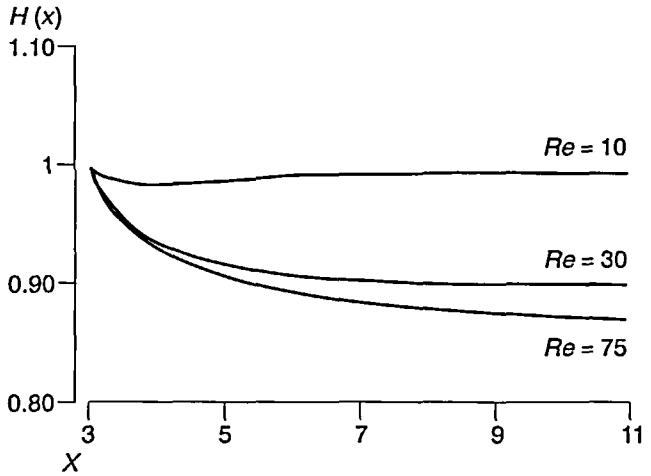

Figure 9 Free surface profiles for Re = 10, 30 and 75

Most polymer liquids are non-Newtonian. The power-law fluids has a simple form of the constitutive equation, namely, the deviatoric stresses are proportional to the rate of deformation tensor but the proportionality coefficients, i.e. the viscosity, is not constant, but is dependent on the rate of deformation tensor as follows:

$$\mu = K\left|\frac{1}{2}\Pi\right|^{(m-1)/2}$$

where Π is the second scalar invariant of the rate of deformation tensor and m is the power-law index. When $m = 1$, the expression describes Newtonian behaviour; when $m < 1$, the fluid is pseudo-plastic (or shear-thinning) and when $m > 1$, the fluid is rheopectic (or shear-thickening). As explained by Tanner *et al.*[25], stability considerations prohibit a negative value of power-law index and $m = 0$ is set as the lower limit which corresponds to the case of plug flow.

The same grid as used for a Newtonian fluid is employed and the boundary conditions are those given previously. *Figure 14* (shown after the References) shows the free surface profiles as a function of the power-law index m in the creeping flow regime. The more shear-thickening a fluid is, the greater the thickness swelling it exhibits. This is to be expected considering the velocity profile inside the die and the degree of flow rearrangement, that occur after emergence from the die. For the shear-thickening fluid, the fluid in the central core region undergoes significant change resulting in severe compression, while the fluid near the die lip experiences pronounced tension. This causes a fluid element to distort and extend in the direction of the free surfaces. Thus, for a shear-thickening fluid, a relatively large thickness swell is obtained.

Finally, similar results for Reynolds number Re = 20 are given in *Figure 15* (shown after the References). Comparing with the jet shapes in *Figure 14*, the jets contract now and the increased power-law index tends to reduce the contraction.

CONCLUSIONS

A novel, efficient finite volume Navier-Stokes method for unstructured grids has been developed. The results demonstrate the capability of employing a finite volume numerical method for solving the free surface extrudate swell problem by direct solution of the continuity and momentum equations using velocity and pressure as the primitive variables. The method has been successfully applied to Newtonian and power-law fluid jets without any difficulty in

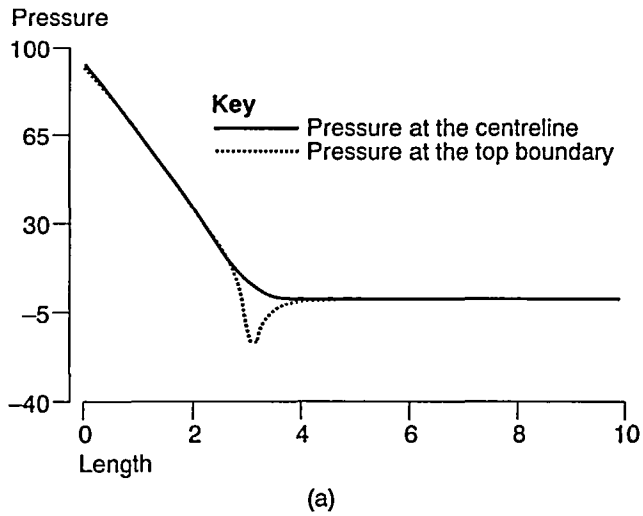

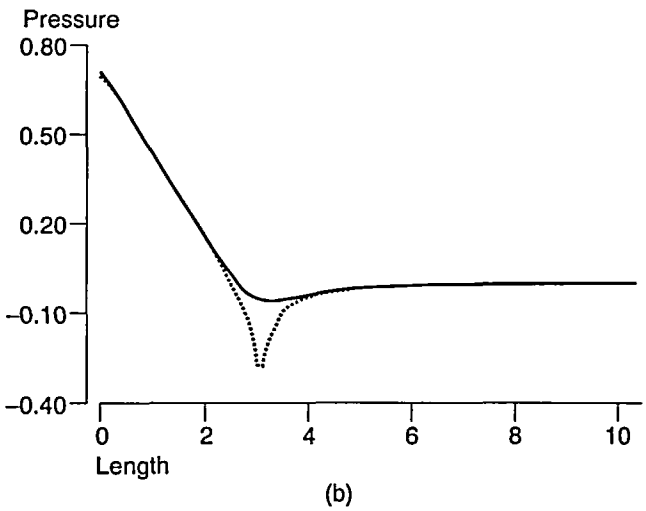

Figure 10a Pressure profiles for die-swell problem. (a) Creeping flow, (b) $Re = 10$

accommodating the free surface by employing an unstructured grid made up of triangles. The current finite volume technique is able to approach the boundary generality of the finite element method.

Numerical solutions for planar jets have been obtained and the numerical predictions based on the present development are in good agreement with the results based on the finite element and the finite difference simulations. Values of the jet swell ratio as function of the Reynolds number, capillary number and power-law index have been presented.

Even though finite element methods are almost exclusively employed for the solution of free surface fluid mechanics problems and attention to finite difference procedures has been virtually abandoned, the present study indicates that finite volume methods on unstructured triangular meshes can be employed without formidable difficulty or complexity and that the method approaches the generality of the finite element method for capturing the boundaries.

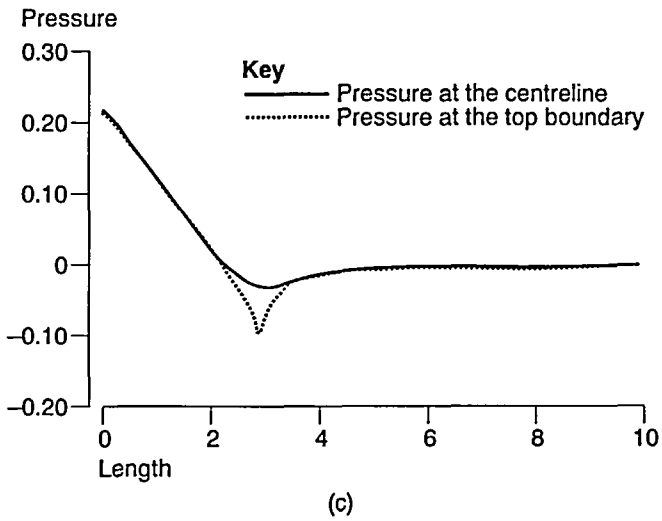

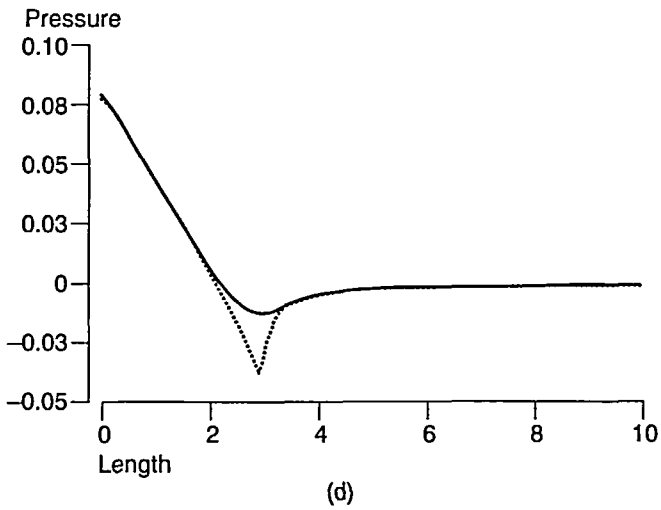

Figure 10b Pressure profiles for die-swell problem. (c) $Re = 30$, (d) $Re = 75$

REFERENCES

1 Goren, S.L. and Wronski, S., The shape of low-speed capillary jets of Newtonian liquids, *J. Fluid Mech.*, **25**, 185-198 (1966)
2 Batchelor, J.J., Berry, P. and Horsfall, F., Die swell in elastic and viscous fluids, *Polymer*, **14**, 297-299 (1973)
3 Nickell, R.E., Tanner, R.I. and Caswell, B., The solution of viscous incompressible jet and free-surface flows using finite-element methods, *J. Fluid Mech.*, **65**, 189-206 (1974)
4 Gear, R.L., Keentock, M., Milthorpe, J.F. and Tanner, R.I., The shape of low Reynolds number jets, *Phys. Fluids*, **26**, 7-13 (1983)
5 Omodei, B.J., On the die swell of an axisymmetric Newtonian jet, *Comput. Fluids*, **8**, 275-289 (1980)
6 Ruschak, K.J., A method for incorporating free boundaries with surface tension in finite element fluid-flow simulators, *Int. J. Num. Meth. Eng.*, **15**, 639-698 (1980)
7 Georgiou, G.C., Schultz, W.W. and Olson, L.G., Singular finite elements for the sudden-expansion and the die-swell problems, *Int. J. Num. Meth. Fluids*, **10**, 357-372 (1990)
8 Dutta, A. and Ryan, M.E., Dynamics of a creeping Newtonian jet with gravity and surface tension: a finite difference technique for solving steady free-surface flows using orthogonal curvilinear coordinates, *AIChEJ*, **28**, 220-232 (1982)
9 Liu, T.J., Yu, T.A. and Cheng, S.H., Finite difference solution of a Newtonian jet swell problem, *Int. J. Num. Meth. Fluids*, **12**, 125-141 (1991)
10 Yu, T.A. and Liu, T.J., An improved finite difference scheme for a Newtonian jet swell problem, *Int. J. Num. Meth. Fluids*, **14**, 495-501 (1992)
11 Chorin, A.J., Numerical solution of Navier-Stokes equations, *Math. Comput.*, **22**, 745-762 (1968)
12 Andersson, H.I. and Kristoffersen, R., Numerical simulation of unsteady viscous flows, *Arch. Mech.*, **41**, 207-223 (1989)
13 Harlow, F.H. and Welch, J.E., Numerical calculation of time-dependent viscous incompressible flow of fluid with free surface, *Phys. Fluids*, **8**, 2182-2189 (1965)
14 Despotis, G.K. and Tsangaris, S., Fractional step method for the solution of incompressible Navier-Stokes equations on unstructured triangular meshes, accepted for publication in *Int. J. Num. Meth. Fluids*, **20**, 1273-1288 (1995)
15 Jameson, A., Baker, T.J. and Weatherill, N.P., Calculation of inviscid transonic flow over a complete aircraft, *AIAA Paper 86-0103*, January (1986)
16 Mavripilis, D.J., Jameson, A. and Martinelli, L., Multigrid solution of the Navier-Stokes equations on triangular meshes, *AIAA Paper 89-0120*, AIAA 27th Aerospace Sciences Meeting, Reno, Nevada, January (1989)
17 Weatherill, N.P., Johnston, L.T., Peace, A.J. and Shaw, J.A., A method for the solution of the Reynolds-Averaged Navier-Stokes equations on triangular grids, *Notes on Num. Fluid Mechanics*, **20**, 418-425 (1988)
18 Jameson, A. and Mavripilis, D., Finite volume solution of the two-dimensional Euler equations on regular triangular mesh, *AIAAJ*, **24**, (4), 611-618 (1986)
19 Whipple, B.A. and Hill, C.T., Velocity distributions in die swell, *AIChEJ.*, **24**, 664-671 (1978)
20 Crochet, M.J. and Kennings, R., Die swell of a Maxwell fluid: numerical prediction, *J. Non-Newtonian Fluid Mech.*, **7**, 199-212 (1980)
21 Omodei, B.J., Computer solutions of a plane Newtonian jet with surface tension, *Comput. Fluids*, **7**, 79-96 (1979)
22 Chang, P.W., Patten, T.W. and Finlayson, B.A., Collocation and Galerkin finite-element methods for viscoelastic fluid flow – II, *Comput. Fluids*, 285-293 (1979)
23 Ahn, Y.C. and Ryan, M.E., A finite difference analysis of the extrudate swell problem, *Int. J. Num. Meth. Fluids*, **13**, 1289-1310 (1991)
24 Georgiou, G.C., Papanastasiou, T.C. and Wilkes, J.O., Newtonian jets at high Reynolds number and high surface tension, *AIChEJ*, **34**, 1559-1562 (1988)
25 Tanner, R.I., Nickell, R.E. and Bilger, R.W., Finite-element methods for the solution of some imcompressible non-Newtonian fluid mechanics problems with free surfaces, *Comput. Meth. Appl. Mech. Eng.*, **6**, 155-174 (1975).

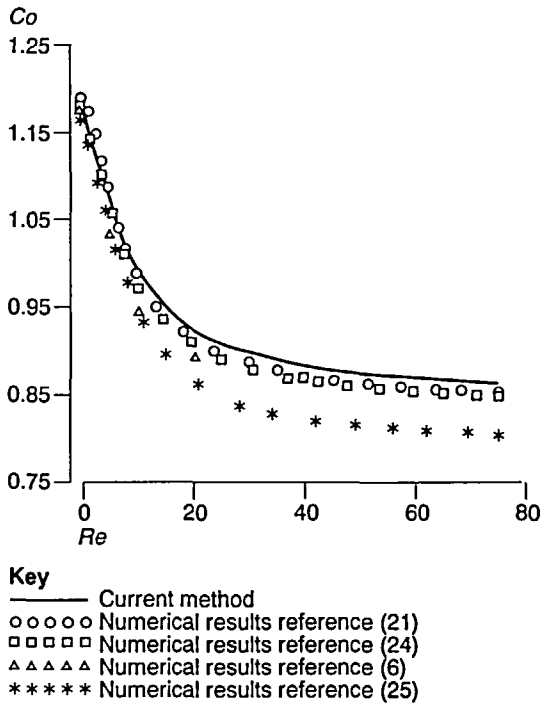

Figure 11 Comparison of the jet swell ratio with previous work

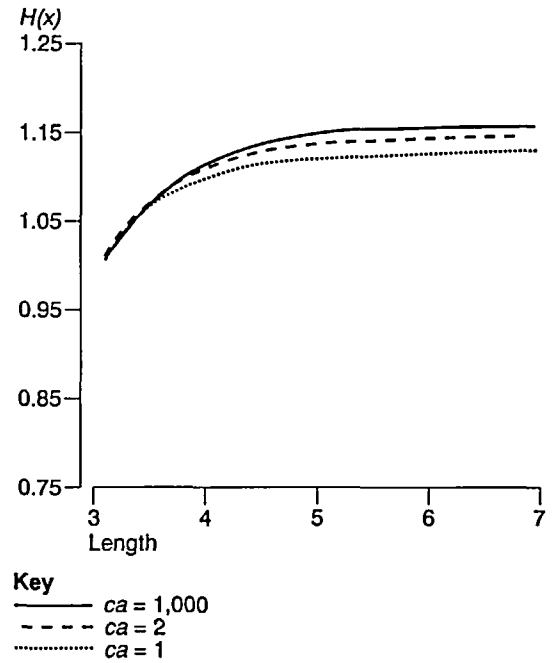

Figure 12 The effect of Cα on the jet free surface at $Re = 1$

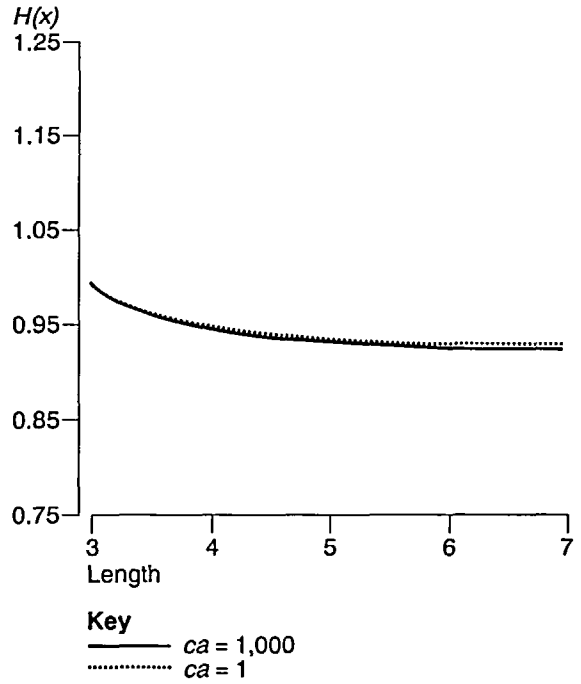

Figure 13 The effect of Cα on the jet free surface at $Re = 20$

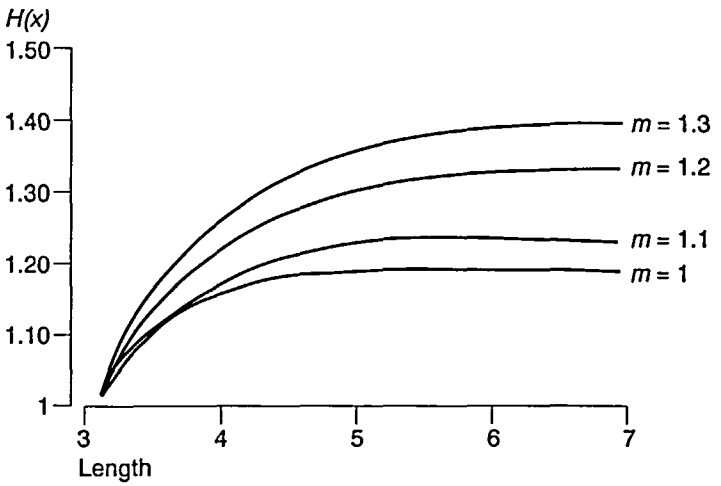

Figure 14 Free surface profiles for creeping flow of the power-law fluids

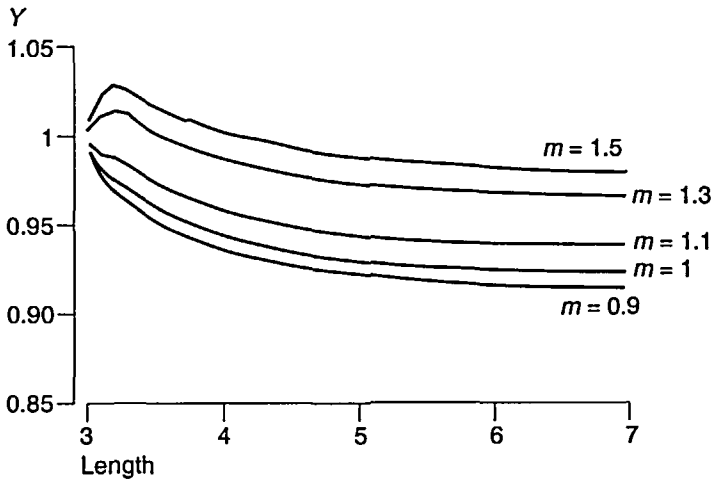

Figure 15 Free surface profiles for power-law fluids and $Re = 20$